4-2015

3D Printing Scintillating Detectors for Field Emission Detection in Niobium SRF Cavities

Alice E. Perrin
College of William and Mary

3D Printing Scintillating Detectors for Field Emission Detection in Niobium SRF Cavities

A thesis submitted in partial fulfillment of the requirement
for the degree of Bachelor of Arts / Science in Department from
The College of William and Mary

by

Alice Perrin

Accepted for HONORS
(Honors or no-Honors)

Wouter Deconinck, Director

Gina L. Hoatson

Gina Hoatson, Physics

Elizabeth Harbron, Chemistry

Williamsburg, VA
April 28, 2015

Abstract

Several methods have been employed to improve detection of field emissions in superconducting radio frequency cavities in electron beam accelerators, but each method has its limitations. We are exploring the possibility of using 3D-printed scintillating detectors for field emission detection because these detectors would allow for in-situ measurements of field emission even in areas in the cavity which have strange geometries. Field emission is the emission of electrons from a surface due to an electrostatic field, most commonly from solid surfaces in vacuum. The superconducting radio frequency (SRF) niobium cavities in Jefferson Lab's Continuous Electron Beam Accelerator Facility (CEBAF) emit field emission electrons during operation and cavity testing. Field emissions limit the field gradient in the cavities and can hinder their performance, so better detection of where the emission occurs will help improve development of cavities for future use. We are replicating the results of the Ron group at Hebrew University, who developed a recipe for scintillating detectors with 30% the efficiency of traditional scintillating detectors, as well as exploring the viability of an additional recipe developed by the Ron group that is thus far untested. We will measure the emission spectra of both detectors and will perform further tests to determine how well the detectors perform over time in vacuum and at low temperatures. If the detectors perform well, we will then explore how they can be best used for field emission detection in the cavities in the CEBAF.

Contents

Background

Field Electron Emission

Jefferson Lab uses niobium superconducting radio frequency cavities to accelerate the electron beam in CEBAF. These cavities accelerate the electron beam by carrying an alternating current (AC) along the cavity walls which create an electromagnetic field. The radio frequency must match the mode of the cavity geometry (see figure 1), and the cavities must be kept at a low, constant temperature to ensure that the cavities continue to superconduct and accelerate the beam in a consistent environment. The superconducting cavities allow for much lower resistance across the inner cavity surfaces compared to radio frequency cavities made out of copper, which allows for much higher field gradients. The critical temperature of niobium is 9.3 K, and the cavities are kept well below this, usually around 2 K, using liquid helium cryomodules. [6]

The electric field present in these niobium SRF cavities causes field emission of electrons from the inner walls of the cavities; these electrons are then accelerated by the radio frequency field until they hit another wall in the cavity and produce Bremsstrahlung rays [5]. The emitted electrons can create an additional heat load in the cavity and this must be regulated by the cryogenic system that keeps the cavities at a low temperature. If the field emitted electrons escape the cavity, they can be accelerated and form a dark current in the accelerator, which can cause activation of the cavity and other accelerator parts. This dark current can also excite higher order modes of the radio frequency field, which can cause electron beam instability and break-up. Current analysis shows that the area of the cavity where the field emitter is located also affects the likelihood that the electron will escape the cavity, and likely affects the rate at which electrons are emitted [3]. Development of future accelerators relies on accurate detection of field emission in the cavities, both during initial testing of cavities when we can access the cavity directly, and while they are in use in the accelerator facility,

at which point we can only measure the field emitted particles passing between cavities.

Jefferson Lab has used several different methods to characterize these field emissions, including correlating existing data on cryogenic heat loads in existing cavities and using Geiger tubes to determine where the electrons are emitted within the cavity, but because Geiger tubes are omnidirectional sensors, this method is difficult to use. Field emitters have also been found during initial testing of cavities in the Vertical Test Area using carbon resistors, but this does not give information on where new emitters are formed during operation in the accelerator. Other methods have included immersing silicon diodes in superfluid helium around SRF cavities [3], which has been done at Jefferson Lab, and NaI detectors with collimators have been used at Michigan State University's National Superconducting Cyclotron Lab [5].

Figure 1: A niobium cavity before installation in an accelerator facility.[1]

3D Printing

To print our detectors, we are using an Asiga Freeform Pico Plus 39 Printer[1], which uses digital light processing to harden a liquid resin layer by layer and create a 3D print. We also use an ultraviolet light curing oven to harden the prints after they are removed from the Asiga. The resin is held in a transparent tray over an ultraviolet light source, and the printer lowers a build platform into the resin until it is microns away from the bottom of the build tray. The ultraviolet light sits below the build tray and shines for a set exposure time which causes the resin to polymerize and harden. The first hardened layer of resin sticks to

[1] `http://newsline.linearcollider.org/images/2010/20100617_dc_1.jpg`

the build platform, and each hardened layer sticks to the layer before it. For each layer, the ultraviolet light is exposed only in areas designated by the build layer cross-section. With this printing method, we can use any liquid monomer that can be polymerized to create our own printing resin and add scintillating components to it, which allows us to print transparent detectors containing scintillating material in any geometry we desire.

The Asiga software allows us to change the settings for ultraviolet exposure time according to how quickly our resin polymerizes. We can also change the burn-in exposure time, which is a longer exposure time used on the first layers of the build that cause them to stick to the build platform. We can also change the type of base on the print depending on the needs of the build; the base comprises the first few bottom layers of the build, which are printed first since the Asiga prints upside down. A full, rectangular base works well for keeping multiple parts together on the same build or giving support to delicate builds. A shadow base is a base platform matching the shape and size of the printed components; it works well for geometry-specific prints and uses less resin during printing. The Asiga Composer software allows rearrangement, rotation, and scaling of imported build components, and allows a maximum print base area of 49.7 mm by 30.8 mm and a maximum print height of 80 mm. Asiga Composer can also generate build supports, which are used to reinforce delicate structures and allow a base connection for any pieces that would not be structurally possible to print otherwise.

Experimental Procedures

Printer Characterization

After installing and calibrating the printer, we printed several test builds to check for precision and consistency in prints using the resin the printer manufacturers provide. This allowed us to ensure that any oddities or issues we had with the printer once we started using

our own resin recipes were not due to inherent issues with the printer or printer software. Our first test print was a replica of the Eiffel Tower (figure 2), which contains many intricate, tiny features; this print was successful and confirmed that the Pico printer was capable of printing to a degree of precision greater than we will likely need for our detectors. A second test print of the leaning tower of Pisa confirmed that the printer handles very precise, intricate features incredibly well. We then began testing the support generation capabilities of the Composer program. Several aspects of the support beams can be altered, including the aspect ratio, contact width, overshoot, and number of sides. The supports are also intended to break off the design easily to avoid damaging the print. We first tested the default settings for the supports by printing a catapult and adding supports with default settings along the fulcrum. Though the catapult itself printed successfully, only one of the eight supports generated appeared to form during the build, and this support did not make successful contact with the fulcrum. This led us to develop more precise tests to see which parameters of the generated supports affect successful support structures.

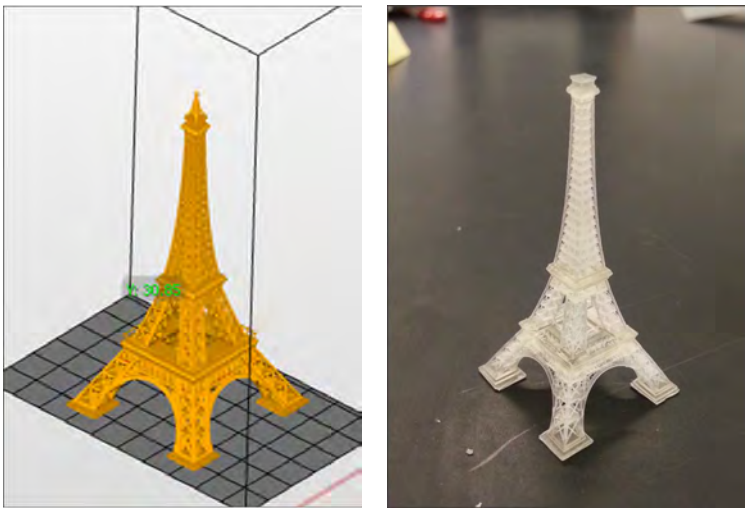

Figure 2: The print of the Eiffel Tower (right) compared to the build file in the Asiga Composer program (left). This print printed without issue (though the tip broke off while cleaning the print) confirming the level of precision achievable with the Pico printer.

The first test we developed featured four rectangular platforms of width 1 mm at heights ranging from 5 mm to 20 mm in 5 mm increments. Each platform is held at these heights by four cylindrical supports with different aspect ratios (fig. 3), and the overshoot of the supports was kept constant at 2 mm. The aspect ratio determines how far the base thickness extends up the support before narrowing to the contact width thickness. The contact width thickness is how wide the support is at its point of contact with the print. For this test, the base width was 3 mm, and the contact width was 1 mm. At each height, the aspect ratios were such that one support would have no widening at the base, and in this case was 1 mm in diameter throughout the column. The next support had a base of 3 mm that tapered to the 1 mm contact width thickness at around about 20% of the height of the support; the next support's based tapered at around 33% of the height; and the last tapered at 50% of the height of the base. This allowed us to observe the extent to which the wider base made for significantly stronger supports.

However, when we printed this supports test, the platforms did not attach correctly to any of the supports, which indicated that there could be other important parameters that we did not consider in the first test. We also questioned whether the thickness of the platforms affected the print, speculating that if they were too thin the first time, it could be difficult for the supports to attach well. We printed the test again with thicker platforms that were 2 mm thick instead of 1 mm, but the supports still did not attach correctly to the platforms. The only platform that attached at all was the 10 mm high platform, and it was attached primarily to the support which had a base width equal to its contact width. This suggested that in future tests, we should set the aspect ratio such that the supports do not flair at the base, but the lack of attachment on the other platforms makes this merely an assumption.

At this point, because of the relative failures of the first supports test, we considered using another program to add supports to the platforms and importing the build as one object, but this option would make the supports too difficult to remove without causing

damage to the print itself.

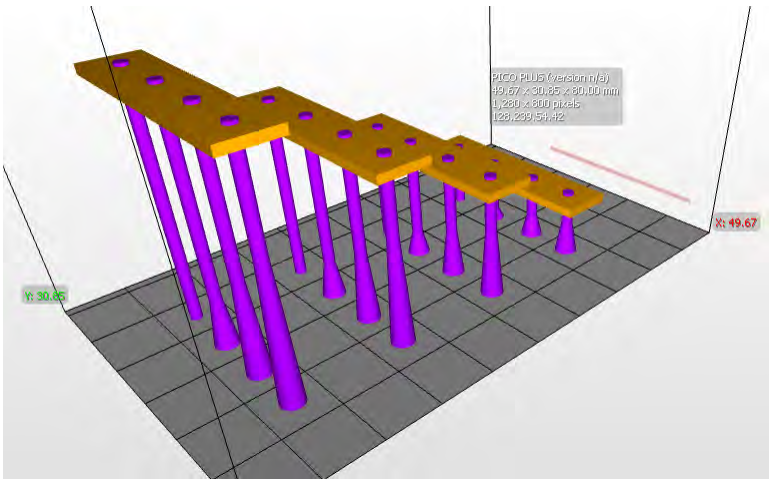

Figure 3: The platforms range from heights of 5 mm to 20 mm in 5 mm increments. Each is held up by four supports, whose aspect ratios are varied to explore the effect of base width on support strength. The overshoot of each support was 2 mm, and the more successful print of this test had platforms with a 2 mm thickness.

We then developed a second test to explore the effect that other support parameters could have on the support-platform attachment. In this test we kept the aspect ratio and platform height constant so that each support was 10 mm high and had equal contact and base width values. We instead varied the contact width (which is the same as the overall support diameter in this case) over a range of 0.5 mm to 2.0 mm in 0.5 mm increments. It also varied the overshoot, which is a measure of how far the support extends into the material. In the first test, the overshoot was 2 mm, which was greater than the thickness of the platforms. We speculated that this may have kept the supports from attaching properly to the platforms, so the second test had five sets of supports with an overshoot ranging from 0.0 mm to 2.0 mm. The design for this test is pictured in figure 4. The physical print from this test suggested that thicker supports with a larger overshoot will print most optimally, and the results from this test also suggest that keeping the contact width of the support equal to the base width results in more effective supports, which agrees with the result of the first

supports test print. However, one disadvantage with large contact widths is that they are more difficult to remove from a print without damaging it, and may leave a larger rough area where it was removed. These tests will be of use later on when we begin printing detectors in more complex geometries that require supports for delicate features. These supports tests verified that the best settings for the generated support parameters are not aligned with the default settings in the Composer software. As calibrating the exposure time of our own fabricated resin proves to be complex, our knowledge of the optimal parameters will drastically reduce the time spent troubleshooting support generation with a less rigorously tested scintillating resin.

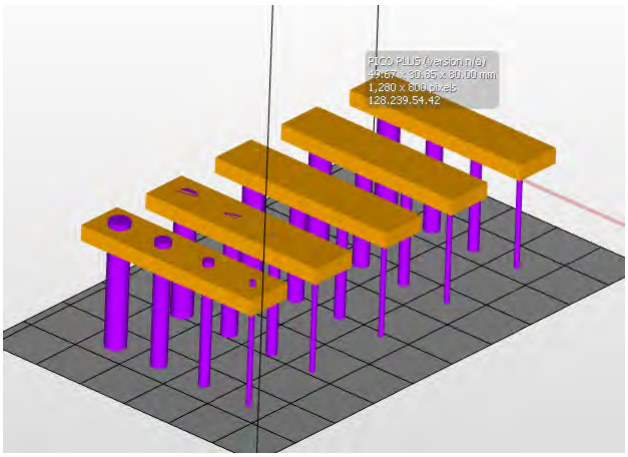

Figure 4: The 2 mm thick platforms are held up by four supports of thickness varied from 0.5 mm to 2.0 mm in 0.5 mm increments. Each platform is supported by a set of supports with the same overshoot, which ranges from 0.0 mm to 2.0 mm in 0.5 mm increments across the build platform.

Resin Fabrication

We have fabricated three batches of scintillating resin for use in the Pico printer. The first two are based on the most successful recipe from the Y. Mishnayot paper [4], which demonstrated 27% efficiency compared to traditional scintillating detectors. These

two batches are referred to as Resin 1.0 and Resin 1.1 throughout this paper, because they are created from the same recipe with different concentrations. This recipe calls for five components. The first component is ethoxylated (15) trimethylolpropane triacrylate, commercially known as SR9035, is a liquid monomer which comprises the transparent liquid base of the resin and can be polymerized with UV light. Ethyl-2,4,6 trimethylbenzoylphenyl phosphinate, commercially known as Lucirin TPO, is a photoinitiator, which encourages polymerization of the monomer under ultraviolet light. The third component, 2,5-Diphenyloxazole, is commercially known as PPO and is a scintillating chemical whose peak emitted wavelength is 303 nm, which is within the ultraviolet light spectrum. The fourth component, 1,4-Bis(5-phenl-2-oxazolyl), also known as POPOP, is a secondary scintillating component; it acts as a scintillator as well as a wavelength shifter, which means that it converts the shorter emitted wavelengths from the PPO into longer wavelengths. These wavelengths peak at 410 nm, which is visible, violet light. It is easier to measure the scintillator emissions in this wavelength range as this is in the peak wavelength detection range of many photo-multiplier tubes, or PMTs. The last component, naphthalene, is an organic compound often used to improve the solubility of other chemicals in a solution; in this case, the naphthalene is aiding the solubility of our scintillating components. However, naphthalene is somewhat volatile; it can degrade over time, and it sublimates at high temperatures. Thus, we are testing this resin recipe along with another recipe developed by the Mishnayot group that omits naphthalene entirely to see how much degradation is visible throughout the testing process.

Our initial goal was only to replicate the results of the Mishnayot paper [4], but through correspondence with the Ron group, we learned that they had developed a new recipe for scintillating resin that did not call for the naphthalene component, and we decided to test this resin in parallel with the first resin recipe. The untested resin is referred to throughout this paper as Resin 2.0. This recipe still uses the PPO, POPOP, and TPO as the primary scintillating component, wavelength shifter, and photoinitiator, respectively, but omits

naphthalene and replaced the SR9035 with another monomer. The new liquid monomer, ethoxylated (30) bisphenol A dimethacrylate is commercially known as SR9036. This resin was fabricated in a similar fashion to Resins 1.0 and 1.1.

The resin fabrication process was relatively simple for both recipes. To fabricate Resin 1.0 and Resin 1.1, we combined the proper concentrations (table 1) of SR9035 and TPO and stirred the solution for 30 minutes in a 60°C water bath. We then added the necessary concentrations of naphthalene, PPO, and POPOP to this solution and stirred for another 60 minutes in a 60°C water bath. For Resin 2.0, we combined the required concentrations (table 1) of SR9036 and TPO and stirred this solution for 30 minutes in a 60°C water bath. We then added PPO and POPOP to this solution and stirred it again in a 60°C water bath. However, likely because of the absence of the naphthalene in the recipe for Resin 2.0, the scintillating components did not dissolve as quickly into the SR9036 solution, and we stirred the solution for 80 minutes instead of 60 minutes to allow for better dissolution of the scintillators. Because these resins are light-sensitive and can be polymerized, we stored them in opaque metal cans to minimize unnecessary exposure to light outside of printing.

The first resin (Resin 1.0 in table 1) we fabricated has a slightly different percentage distribution of the chemical components from the Mishnayot recipe due to differences in our initial calculation methods, and so it was used only for exposure time calibration in the Asiga printer. The second resin (Resin 1.1 in table 1) used the same chemical distribution as Mishnayot's most efficient recipe and was used for both calibration purposes and as the printing resin for our first detector. Resin 1.1 is the most efficient recipe from the Mishnayot paper, but because of the volatility of the naphthalene, we were interested in testing not only the original recipe, but the unpublished recipe (Resin 2.0) provided to us by the Ron group.[4]

	Resin 1.0	Resin 1.1	Resin 2.0
SR9035	85.35%	82.92%	–
SR9036	–	–	97.92%
Lucirin TPO	0.43%	0.50%	0.50%
Naphthalene	12.87%	15.00%	–
PPO	1.29%	1.50%	1.50%
POPOP	0.07%	0.08%	0.08%

Table 1: Concentrations of chemicals in each resin recipe. Resin 1.0 and Resin 1.1 are fabricated from the same recipe; only Resin 1.1 was used for all testing purposes after the initial printing calibration. Resin 2.0 is thus far untested.

Resin Printing and Calibration

These resins each require a specific amount of exposure to the ultraviolet light source in the Asiga printer in order to polymerize correctly. If a layer is overexposed, the surrounding edges of the exposed region may also begin to harden, and the print will be non-uniformly thicker (figure 5). If a layer is underexposed, the resin will not harden completely and may not attach to the previous layer correctly. This can lead to a build-up of hardened resin on the build tray and the print will taper off in size; for example, our underexposed cylindrical prints looked like cones as each layer failed to adhere completely to the one above it (figure 5). The exposure time of the clear, non-scintillating resin that came with the Asiga printer is 1.393 s/layer when the layer thickness is 0.025 mm thick. Mishnayot's paper confirmed that their 3D printed detectors were more efficient when printed with thinner layers (0.025 mm versus 0.075 mm), so we optimized exposure time for 0.025 mm layers as well.

There were several variables that complicated the calibration process. For calibration of Resin 1.0 and 1.1, we began by printing cylindrical prints with height 8.57 mm and diameter 9.66 mm with an ultraviolet light exposure time at 1.393 s/layer and altered the time for each successive print by 0.1 s/layer. The first print appeared to have excess resin towards the bottom edges of the intended shape, but since the sticking resin near the bottom may have been a side effect from the burn-in layers, we increased the exposure time incrementally

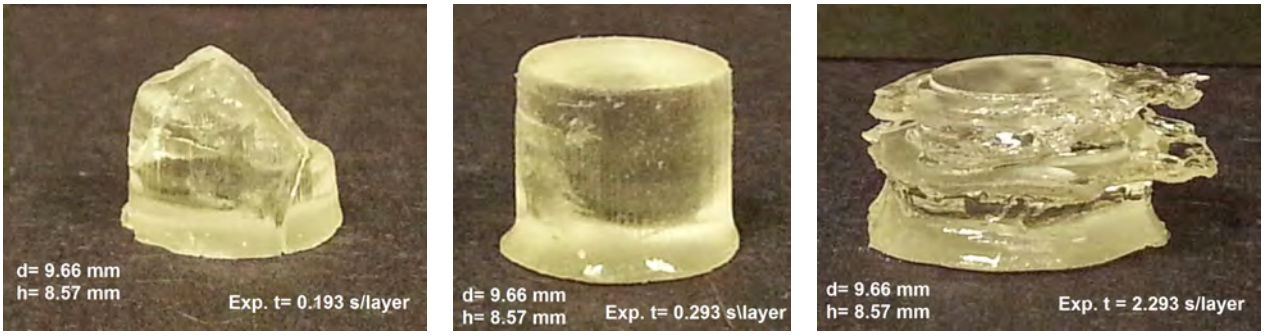

Figure 5: Three prints with Resin 1.0. The left is underexposed, evident by the tapering at the top of the cylindrical print. The center is correctly exposed. The right is overexposed, evident by the large, irregular rings of resin on the print as well as the overall print width, which is much larger than the intended width of 9.66 mm.

by 0.1 s/layer until the prints were obviously printing wider than expected across the entire print to confirm that it was overexposed. The burn-in layers are the bottom layers of a print which are exposed for a much longer time to the UV light in order to make them stick to the build platform. Because these layers are so heavily exposed, they can turn out thicker than the expected shape, and can cause distortion at the bottom of prints.

Once we confirmed that the prints were overexposed, we lowered the exposure time in 0.1 s/layer increments from 1.393 s/layer. Upon reaching an underexposed print, we then printed at exposure times between that time and the next lowest time, in this case, between 0.193 s/layer and 0.293 s/layer, and iterated until we reached a print that was exposed correctly. For the 9.66 mm diameter prints, the lowest functional exposure time was 0.268 s/layer. We define the lowest functional exposure time as the least amount of time the layers can be exposed while still maintaining the integrity of the print; we wanted to find this because at this exposure time there is the least risk for overexposing or warping the print. However, there appeared to be a range of exposure times over which the effects of overexposure appeared to be minimal; for example, the 9.66 mm diameter prints were not noticeably overexposed at 0.393 mm though the minimal functional exposure time is at

0.268 mm. The full range of exposure times we explored at this diameter can be seen in figure 6, where the effects of overexposure can be more clearly seen through the spectrum of increasing exposure times. Figure 6 also shows how little the prints changed between the minimum functional exposure time, 0.268 s/layer, and 0.393 s/layer, demonstrating that there is an acceptable range of exposure times over which the prints can be printed without noticable distortion.

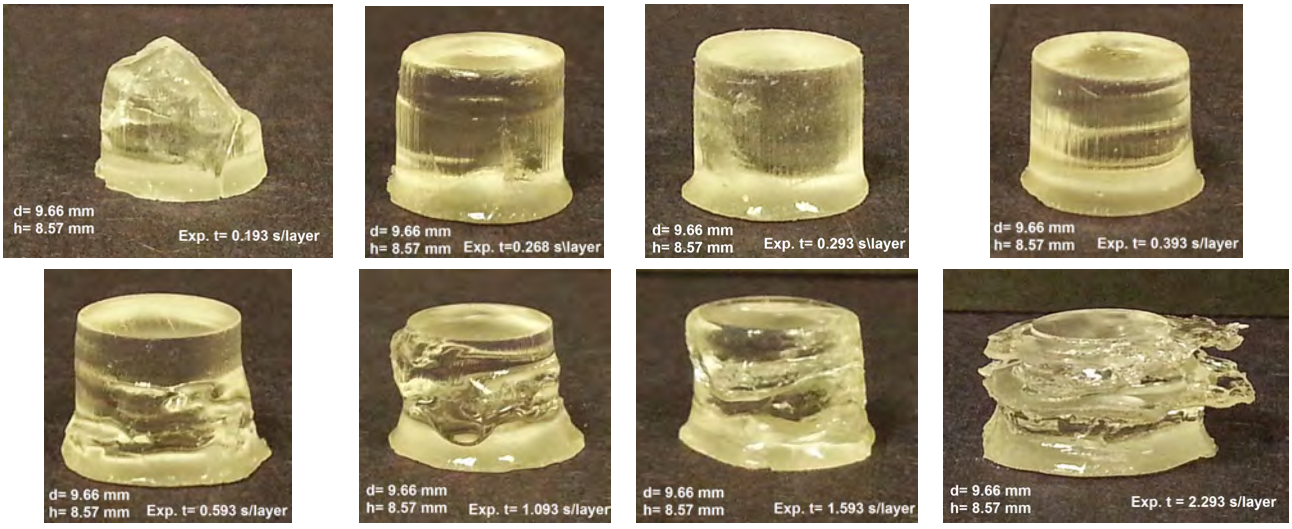

Figure 6: The results of a range of exposure times for Resin 1.0 and Resin 1.1. Evidence of overexposure becomes clear at t=0.593 s/layer and becomes more dramatic as the exposure time is increased.

After finding the lowest functional exposure time for a the 9.66 mm diameter prints, we then increased the diameter of the prints to confirm that this exposure time was sufficient for all print sizes, but the print with height 8.57 mm and diameter 19.32 mm (twice the first print diameter) was very underexposed, and further calibration was necessary. This suggested that the minimum functional exposure time is dependent on the size of the features of the prints; however, because of the relatively unchanging characteristics of the prints within a few milliseconds of the exposure time for the 9.66 mm diameter prints, it is possible that a higher exposure time for thicker prints would not necessarily have a negative effect on the

integrity of thinner components in a print with strange geometries (for example, in a print where the features taper off). We found that the minimum functional exposure time for a 8.57 mm tall cylinder with diameter of 19.32 mm was 0.343 s/layer. Upon observing that the exposure time increased with diameter, we also attempted prints with the same diameter but twice the height (17.14 mm) to see if the height of the builds is a factor in the exposure time calibration, but our prints confirmed that height of the print had no effect (figure 7).

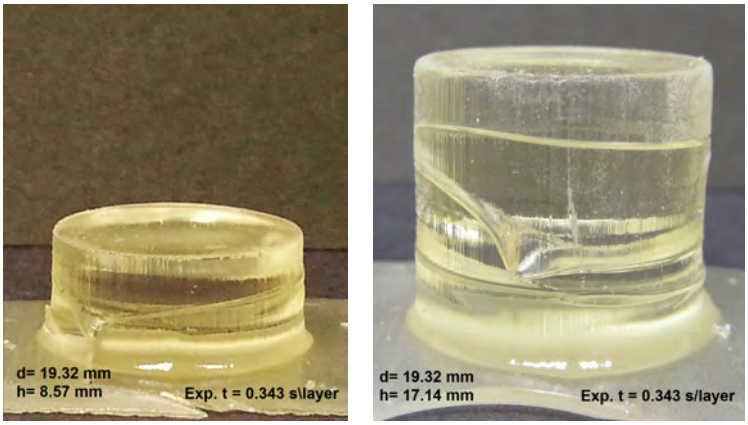

Figure 7: Two prints with Resin 1.1 which have the same diameter, but the print on the right is twice as tall. These prints showed that there was no variation in minimum functional exposure time due to print height.

At this stage in our calibration, we also explored the possibility of decreasing the burn-in exposure time in order to decrease distortion of the bottom layers of the prints. The default burn-in exposure time is 8.743 s on the Asiga, but because our recipe for Resin 1.0 and 1.1 required a much lower exposure time than the non-scintillating printing resin, we speculated the burn-in time could also be scaled down to reduce distortion. At the higher burn-in exposure times, the excess resin surrounding the burn-in layer is also extremely brittle, and we hoped that by lowering the burn-in time we could avoid the non-uniform cracking of the bottom layers. However, we found that at the point when the burn-in layers no longer cracked upon removal from the build platform, the prints were at risk of detaching from the platform during the printing process, particularly with thicker, taller prints that

are heavier. For the purposes of continuing with the calibration of the print exposure time, we defaulted back to the higher burn-in exposure time to guarantee that prints would stick to the build platform.

The final diameter for which we calibrated a minimum functional exposure time was 25 mm, which is the same diameter as the type of photomultiplier tube that we may later use to measure the emissions of our detectors [2]. This larger diameter requires a larger exposure time, 0.393 s/layer, as expected from our previous results. The samples we have printed with Resin 1.1, which will be used for further testing of the efficiency and durability of this resin recipe are cylinders with a diameter of 25 mm and a height of 30 mm. Figure 9 shows how the minimum functional exposure time varied with the diameter of the prints, which appeared to be a linear relationship.

Throughout the calibration process for Resin 1.0 and 1.1, we cured each print in the UV curing oven for 20 minutes. This process hardens the prints, but over-curing can cause the prints to become brittle and may cause cracking, so it is important to pay attention to the prints after curing to ensure that cracks do not appear over time. We cured the smaller prints for 20 minutes under the lamp, and we cured some of the larger prints for 30 minutes because of their increased thickness. However, some of the prints, both those cured for 20 minutes and those cured for 30, have developed cracks over time (i.e. that were not present immediately after curing) that penetrated the prints internally. Evidence of this cracking can be see in figure 8. Repeat prints of the print seen in figure 8 were cured for 5 minutes and also developed internally penetrating cracks, suggesting that the curing process itself is unnecessary for this resin recipe. A final print of the 25 mm diameter cylinder was not cured after printing, and thus far has not developed cracks, so this is tentatively a solution we will employ for prints of all sizes printed with Resin 1.1. This result, as well the as finalized exposure time, can be found in table 2.

Because the calibration of Resin 1.0 and 1.1 demonstrated that the minimum functional

Figure 8: Large internal cracks evident on a print with PMT-compatible dimensions. These cracks developed days after the print was printed and cured for 20 minutes with an ultraviolet lamp. Repeated prints cured for only 5 minutes also developed internal cracks similar to these.

exposure time is greater for larger prints, we began calibration of Resin 2.0 with cylinders with a diameter of 19.32 mm and height of 8.57 mm instead of the smaller dimensions of the initial test prints used for Resin 1.0 and 1.1. We first printed these cylinders with an exposure time of 0.393 s/layer, the optimal exposure time used for Resin 1.0 and 1.1, but found that the prints were severely underexposed (figure 10). Because of the extent of underexposure, we increased the exposure time in larger increments, by 0.4 s/layer, until we had printed an overexposed print, and then printed at a time halfway between that time and the next highest exposure time, which in this case were 1.993 s/layer and 1.593 s/layer. However, it was quickly apparent that these prints were being affected by factors other than exposure time. The print at 1.193 s/layer had a typical appearance of underexposure (figure 11). However, prints in the 1.393 s/layer to 1.7.393 s/layer range appeared both underexposed and overexposed at the same time. These prints were bullet shaped, and the layers that didn't stick to them was found on the bottom of the build tray, as we would expect for an underexposed print. However, the extent to which the 1.993 s/layer print was overexposed,

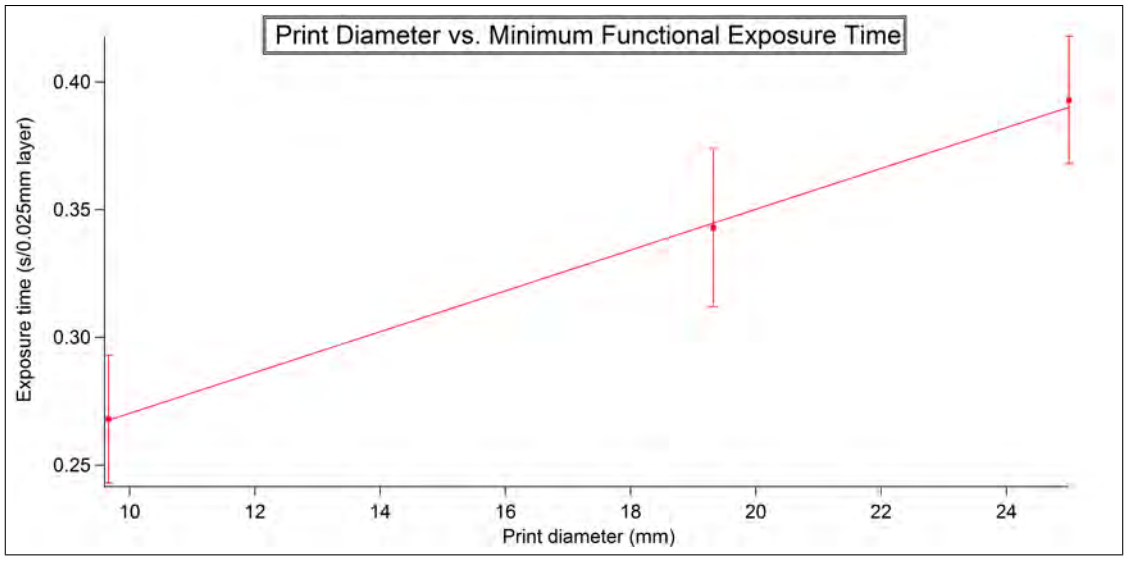

Figure 9: There is a linear relationship between minimum functional exposure time and print size for Resins 1.0 and 1.1. Larger prints with smaller features must still be printed with higher exposure times to ensure proper printing.

and the thickness and wide diameter of the detached layers found on the bottom of the tray suggested that the prints were indeed being overexposed (figure 12). From this curious issue, we speculated that there was something preventing our layers from sticking together as they should. Our first solution was to strain the resin with a fine mesh strainer, which would remove any particles of resin that were at all solidified.

We strained Resin 2.0 to remove these particles of partially or fully exposed resin from the tray, because solid particles in the resin can interfere with the prints. We found an unusually high amount of semi-polymerized particles. Particularly when prints are overexposed, it is more likely that resin surrounding a build will become semi- or fully-polymerized, but because it was not the focus of the ultraviolet light, it does not always attach directly to the build. We had to strain Resins 1.0 and 1.1 occasionally to account for this issue, but the amount of particles filtered out by the mesh strainer were relatively small compared to the amount filtered from Resin 2.0. This also suggested that our prints, though appearing to have the shape of underexposed prints, were in fact being overexposed during printing. How-

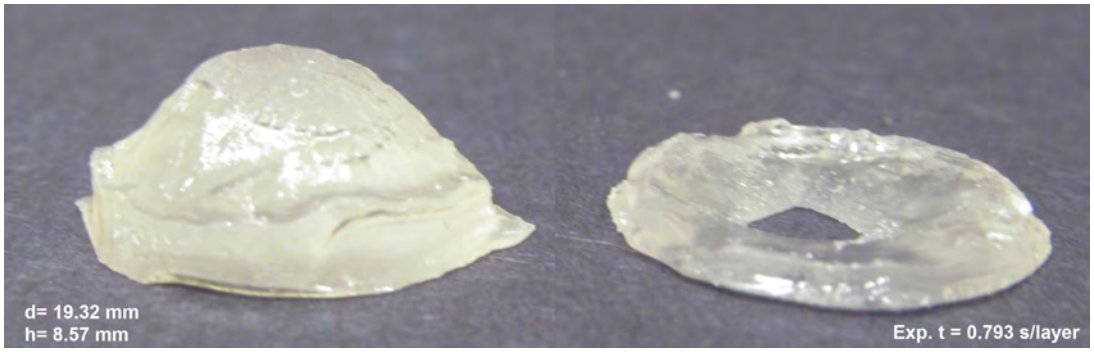

Figure 10: At an exposure time of 0.793 s/layer, this Resin 2.0 print was underexposed. This is evident from the bullet shape of the print (left) and from the size of the ring left on the resin tray, which is roughly the same diameter as the print. If the diameter of the print and the ring are the same, it shows that the ring is part of the build that did not stick correctly to the print and instead built up on the resin tray.

ever, the prints printed after our first straining of the resin were still not printing correctly, so removing the particles may have only treated a symptom of the problem.

The next potential issue we addressed was the temperature of the printing resin. The SR9036 monomer used as the base for Resin 2.0 has a suggested storage temperature range of 2°C to 8°C, and leaving the resin in room temperature conditions for extended periods of time while printing may have negatively affected the performance of the resin and changing its chemical properties. When we were not printing, wee began storing our Resin 2.0 in a refrigerator, and only printed with it for a few hours at a time to ensure that it did not stay in room temperature conditions for extended periods of time. However, perhaps because of the amount of time the resin initially spent at room temperature, the prints were still not forming correctly. The prints from after we began refrigerating Resin 2.0 did show some overall improvement, though, as these prints had flatter tops and appeared to taper only on the top edges of the cylinders. We are in the process of fabricating another batch of recipe 2.0 (table 1) and will keep this resin refrigerated at all times when it is not in use. If the refrigeration is the only issue, prints with the new resin using the method of constant refrigeration may allow us to see positive calibration results very quickly. For now, based on

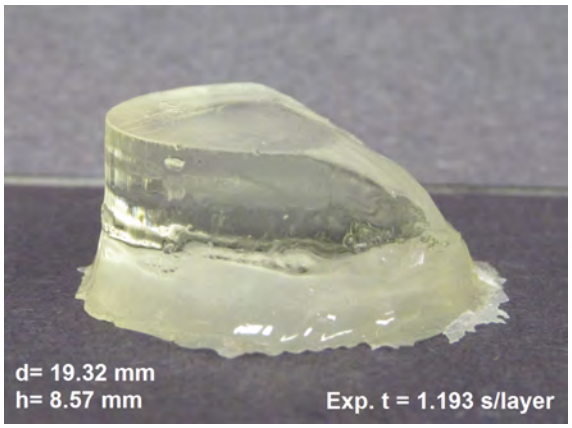

Figure 11: At an exposure time of 1.193 s/layer, this Resin 2.0 print was still underexposed. This built appears to be very close to a correct exposure because one side of the cylinder has printed correctly, and there is tapering indicative of underexposure on the other side.

the initial prints with Resin 2.0 (which were printed right after fabrication, and thus were not affected by the refrigeration issue) and the size of the overexposed detached rings on later prints, we can at least determine that the exposure time for Resin 2.0 is in a range between 1.193 s/layer and 1.593 s/layer. This result can be found in table 2.

The two resins evidently require much different exposure times, curing times, and storage methods for proper printing with the Asiga, and these findings can be found in table 2.Because of the difficulties we have faced with the calibration of Resin 2.0, the calibration step in this project is ongoing. However, because of our successful prints with Resin 1.1, we have begun work on the next step in the project, which is testing the efficiency of our prints, though our focus is still on calibrating the exposure time for Resin 2.0. In the next step of testing, we will measure the emission spectra of these prints to determine their overall efficiency and whether they function similarly. These detectors were printed in cylindrical shapes because a circular face will align the ends of the detectors with the face of a PMT. Commercial scintillating detectors are typically rectangular prisms; we will be able to account for this difference during the measurement of emission spectra to determine the efficiency of our detectors.

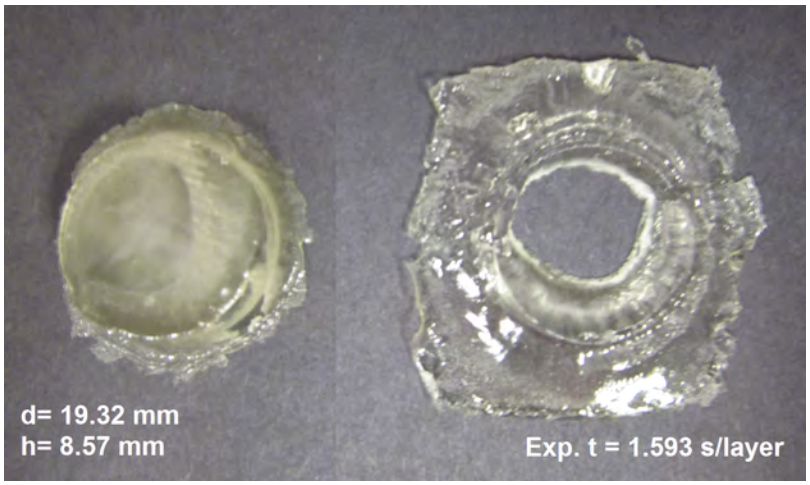

Figure 12: At an exposure time of 1.593 s/layer, this Resin 2.0 print appears both overexposed and underexposed. The print (left) tapers like an underexposed print, but the ring of unattached polymerized resin stuck to the resin tray is much wider than the diameter of the print diameter. The ring is being overexposed during the printing process and mimicks the wide, irregular rings found on overexposed prints where attachment is not an issue.

Gathering Emission Spectra

Our primary method for testing the utility and durability of our printed detectors will be to measure the emission spectra of the scintillating detectors with a monochromator. We will expose our detectors to a low energy radiation source in order to stimulate the scintillating compounds in the detectors and cause them to emit light. The radiation source, our detector, and the opening of the monochromator will all be contained in a blackbox to ensure the emission spectra are measured accurately. We are currently in the process of procuring a monochromator for this setup and building a blackbox suitable for our needs. A diagram of this setup can be seen in figure 13.

Using a monochromator to measure emission will allow us to not only measure the total amount of scintillator emission from the detectors for a given amount of radiation exposure, but also determine the emission spectrum of each detector. Because the POPOP scintillating component shifts shorter wavelengths into the violet light range, we expect to

	Resin 1.0	Resin 1.1	Resin 2.0
Exposure Time (for a 0.025 mm layer)	0.393 s/layer	0.393 s/layer	1.193–1.593 s/layer (range)
Curing Time	0 min	0 min	30 min
Notes	Not used for efficiency tests		Resin must be refrigerated when not in use

Table 2: Final calibrated exposure times, curing times, and additional requirements/comments for each resin recipe. Because Resin 2.0 is still proving difficult to print correctly, we can at present only provide a range in which the most optimal exposure time lies.

see a peak in this area on the spectra. However, other areas of the spectra may allow us to normalize our emission data with the emission spectrum of a traditional scintillating detector in order to determine the relative efficiencies of our detectors, which is necessary because of the geometrical differences between our detectors and commercial detectors. In areas of the spectra where we see little emission for all of the detectors, as well as a similar shape to the emission spectra in these areas on our detectors' emission spectra and the spectrum of commercial detectors, we can normalize our own data to fit the commercial detector's data in an area of the spectrum where we see these similarities. By superimposing our normalized emission spectra data on the commercial detector's spectrum, we can look at regions where the intensity of emissions are vastly different and determine how much more light is being emitted by the commercial detectors in those regions than by our detectors. This will give us an estimate for the overall efficiency of our detectors. This will also give us an opportunity to see how the efficienty of Resin 2.0 compares to the efficiency of Resin 1.1, because Resin 2.0's relative efficiency has not been determined yet. This step in the project is ongoing as well, as we are currently working to assemble the setup seen in figure 13.

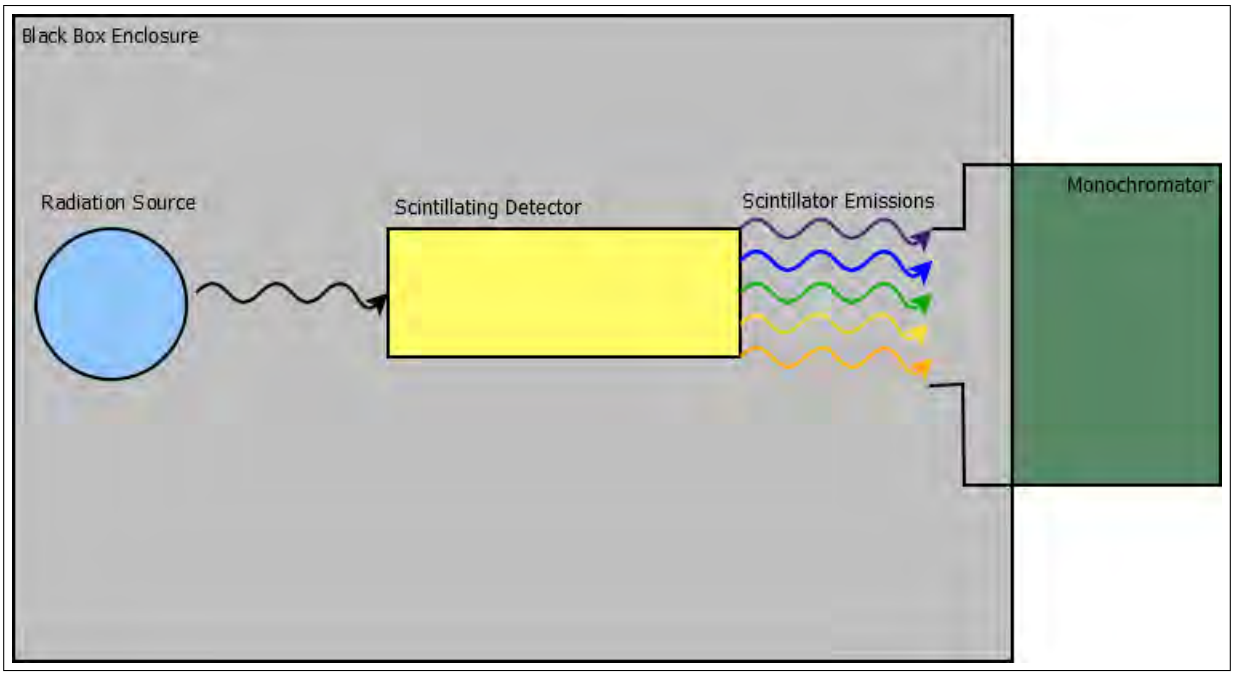

Figure 13: The setup for the initial emission and efficiency testing of our detectors.

Future Work

The next step after gathering emission spectra and analyzing the efficiency of the detectors will be to study how the detectors react to being held in vacuum conditions and at low temperatures. Our initial method to test the detectors' durability in these extreme conditions will be to submerge the detectors in a low temperature, vacuum environment for some period of time, and then gather emission spectra from the detectors again at room temperature (in the same monochromator setup seen in figure 13) to see whether they have lost any ability to scintillate or detect radiation. There may also be obvious signs of degradation of the detectors if the vacuum or low-temperature conditions cause them to discolor or crack. For this step, we have already machined a simple clamp to hold our printed detectors in place on a dewar used in the Vertical Test Area (VTA) at Jefferson Lab, which is where the niobium cavities go through testing at low temperatures. Our two kinds of detectors may react differently to this testing because of the presence of naphthalene in Resin 1.1, so

this step may also eliminate one of our recipes if one behaves vastly better or worse than the other under these new conditions. If the detectors react similarly to the vacuum and cold conditions, whether it be with no degradation at all, extreme and immediate degradation, or a steady decline in scintillating performance over time, we may need to revisit the resin recipes and determine what components we can add or tweak to increase the stability of our detectors over time and under extreme conditions.

If the detectors perform well after being held in these conditions, we can then develop tests to determine how well they perform in the presence of these conditions. Instead of measuring emission spectra generated by a radiation source, we would submerge the detectors in the dewars again, but we would this time include some way to measure the detectors' emissions. As niobium cavities develop field emitters during production and testing, there would be field emission in the dewar that would stimulate our detectors and cause scintillation. The success of this experiment would determine whether our detectors could work as a new form of field emission detection during new cavity testing; if they were a viable option, we could then print the detectors with more complex geometries in order to fit them in the concave areas along the outer cavity walls (figure 1). As field emitters appear to form along these curves within the cavity [3], this area along the outside of the cavity will be the best place to put a detector for maximum emission detection. If the detectors do not perform well under low temperatures, they may still be viable for use in emission detection in the accelerator facility. In CEBAF, each niobium cavity is contained within a cooling chamber that keeps it at a low temperature, so we would not be able to place detectors directly around the cavities in this area. However, the joints where each niobium cavity is joined to the next are uncovered by these chambers, and placing detectors around these joints would allow us to measure field emitted electrons that strike the wall of the joint as they pass through. Detecting the extent of the field emission within the accelerator enclosure is important for determining the additional heat load caused by the emissions, which must be compensated

for in the cooling chambers.

Conclusion

This project started as an attempt to replicate the results found by the Ron group in the Mishnayot paper [4]. However, it expanded with the addition of a second resin formula, and the current focus of the project is the successful calibration of this resin in order to print detectors that we can begin probing with a radiation source in order to obtain emission spectra. At this point, we are also in the process of assembling all the components of the set-up needed for measuring the emission spectra of the detectors. Though I will conclude my work on this project shortly, the testing and trial phases of the project will be continued by other undergraduates who will take over this project. Since we are in the early stages of testing these detectors, it is likely that in the coming months we will determine what can be done with the detectors we have created in their current state, and what can be done to improve them for future use. However, there is still much work to be done before these detectors can be considered viable for use in field emission detection in the niobium cavities used at Jefferson Lab.

Acknowledgements

I would like to thank the people who have helped me throughout the course of this project, including my advisor Wouter Deconinck for overall project support and consultation. This project required a lot of completely new supplies, sometimes things that were not apparent in the beginning of each step of the project but became necessary to continue on, and Wouter's insight into what we needed and the speed with which he made sure we got it was incredibly helpful. A huge thank you as well to Will Henninger for helping me out in the machine shop, Valerie Gray for her help with troubleshooting the Pico 3D printer, fine tuning the printing process, and getting clear pictures of the prints, Janet Hopkins for providing constant consultation throughout my first resin fabrication, and Michael Kelley for the use of his lab and equipment.

References

[1] Asiga. Pro Professional Desktop 3D Printers. `https://www.asiga.com/media/main/files/Pico\%20Brochure\_us\_en.pdf`, 2013. Online: Accessed 2015-4-1.

[2] Hamamatsu. Head-on PMT Photosensor Modules H10492 Series. `http://www.hamamatsu.com/resources/pdf/etd/m-h10492e.pdf`. Online: Accessed 2015-4-10.

[3] Li, Y. et al. Research on Field Emission and Dark Current in ILC Cavities. *SRF2013 TUIOA06*, 2013.

[4] Mishnayot, Y. et al. 3D Printing of Scintillating Materials. *arXiv preprint arXiv:1406.4817*, 2014.

[5] Musser, S. et al. X-Ray Imaging of Superconducting RF Cavities. *SRF2005 TUP27*, 2005.

[6] Padamsee, Hasan S. Superconducting Radio-Frequency Cavities. *Annual Review of Nuclear and Particle Science*, 2014.